STATIONARY HOMOGENEOUS RAYLEIGH-TAYLOR TURBULENCE IN A TRIPLY PERIODIC BOX

Aaron A. Nelson
Department of Mechanical and Civil Engineering
California Institute of Technology
1200 E. California Blvd., Pasadena, CA 91125
aanelson@caltech.edu

Guillaume Blanquart
Department of Mechanical and Civil Engineering
California Institute of Technology
1200 E. California Blvd., Pasadena, CA 91125
g.blanquart@caltech.edu

ABSTRACT

A novel framework, homogeneous buoyant turbulence (HBT), is proposed as a means of modeling the fine turbulence structure found in Rayleigh-Taylor (RT) instabilities. The methodology builds on an existing framework that leverages self-similarity to produce a statistically stationary RT mixing layer (SRT). By homogenizing the flow variables through analytical transformations, source terms are derived which, when applied in a triply periodic box domain, produce a homogeneous stationary flow. HBT statistics, including probability density functions, energy spectra, and velocity gradient variances, show a high degree of fidelity to far more expensive direct numerical simulations (DNS) of the full RT instability.

MOTIVATION

Rayleigh-Taylor instabilities are a feature of several flows of scientific interest, including atmospheric flows, stellar interiors, supernovae, and inertial confinement fusion. They are characterized by a heavy fluid lying above a light fluid within a gravitational field. Disturbances in the interface between the fluids are induced to grow by the vertical pressure gradient, eventually forming a turbulent mixing layer. At late times, the layer has been observed to grow in a manner predicted by self-similarity analysis (Ristorcelli & Clark, 2004).

DNS of practical RT flows is prohibitive, and cheaper large eddy simulations are not yet reliable in the absence of subgrid-scale models experimentally validated for buoyant flows. Nonetheless, it is possible to resolve a canonical problem, termed a temporally evolving RT layer (TRT), where two semi-infinite reservoirs of heavy/light fluid are initially separated by a perturbed interface. They can be characterized by two parameters, a bulk Reynolds number and Atwood number:

$$\mathrm{Re} = \frac{h\dot{h}}{\nu}, \qquad \mathrm{At} = \frac{\rho_H - \rho_L}{\rho_H + \rho_L} \tag{1}$$

where h is some metric for the layer height, and ρ_H and ρ_L are the densities of the heavy and light fluids. One of the largest studies of this kind was the DNS of Cabot & Cook (2006), which reached 3072^3 grid cells at the latest stage of the layer's growth. Unfortunately, TRT requires a growing computational grid to contain the growing mixing layer. Moreover, effects of the initial conditions persist at late times, and data at the largest Reynolds number are limited to a single timestep.

These numerical obstacles have motivated the development of frameworks to reproduce the statistics of RT instabilities in flows with simplified computational domains. Both homogeneous decaying buoyant turbulence (Livescu & Ristorcelli, 2007) and stationary inhomogeneous buoyant turbulence (Chung & Pullin, 2010) have been induced in periodic box domains. Carroll & Blanquart (2015) produced a periodic box buoyant flow that is both stationary and homogeneous by adding source terms to the Navier-Stokes equations. However, the forms of these terms lack physical justification. Goh & Blanquart (2025) proposed SRT, where the lengthscales of the TRT equations are rescaled by their expected self-similar growth to produce a stationary TRT.

To date, a framework to model RT turbulence which is fully homogeneous, is stationary in time, and generates turbulence through a physics-derived mechanism has not yet been proposed. This work presents homogeneous buoyant turbulence (HBT), which satisfies each of these criteria. Here, its formulation is outlined, and its fidelity to TRT is validated.

STATIONARY HOMOGENEOUS RT FLOW

The canonical TRT is governed by continuity, a momentum equation, and a transport equation for a scalar Y:

$$\frac{\partial \rho}{\partial t} + \frac{\partial \rho u_j}{\partial x_j} = 0, \tag{2}$$

$$\frac{\partial \rho u_i}{\partial t} + \frac{\partial \rho u_i u_j}{\partial x_j} = -\frac{\partial p}{\partial x_i} + \frac{\partial \tau_{ij}}{\partial x_j} + \rho' g \delta_{1i}, \tag{3}$$

$$\frac{\partial \rho Y}{\partial t} + \frac{\partial \rho u_j Y}{\partial x_j} = \frac{\partial}{\partial x_j}\left(\rho D \frac{\partial Y}{\partial x_j}\right) \tag{4}$$

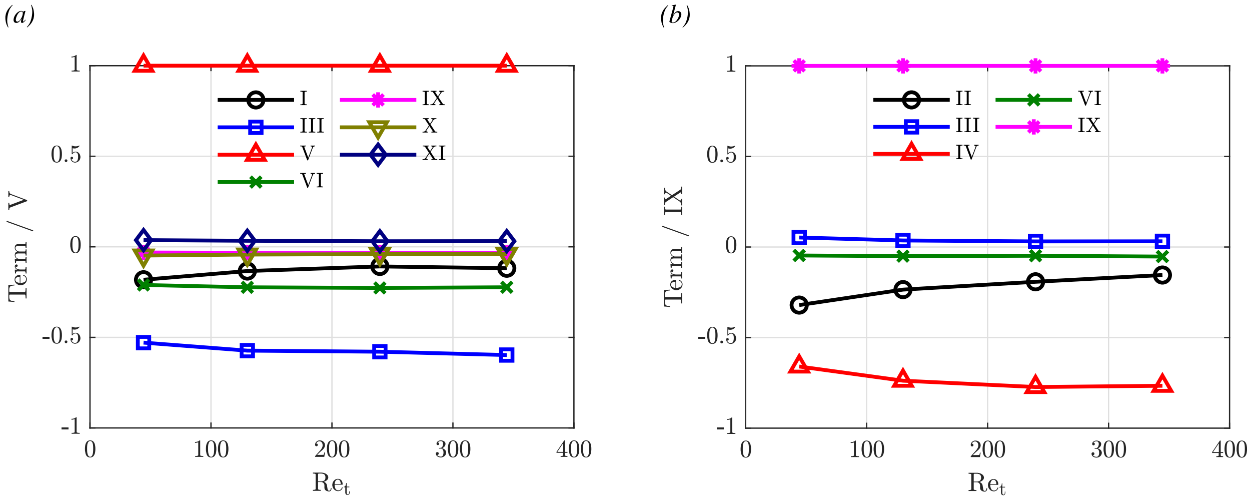

Figure 1: Terms in budgets for (*a*) transformed kinetic energy and (*b*) the transformed scalar variance versus turbulent Reynolds number, evaluated at the midplane of SRT cases G1-4 of Goh & Blanquart (2025).

where u_i is velocity, ρ is density, p is pressure, ν is the kinematic velocity, τ_{ij} is the viscous stress tensor, g is gravitational acceleration, and D is the diffusivity of Y. Y represents either the mass fraction of the lighter of two mixing fluids or a non-dimensionalized temperature, and can be related to the density through an ideal gas equation of state of the form:

$$\rho = \frac{1}{\alpha Y + \beta} \tag{5}$$

The flow dynamics are independent of the values of α and β if ρ_L and ρ_H are held fixed. For simplicity of the present analysis, it is assumed $\beta = 0$. Throughout this analysis, overlines indicate ensemble averages and primes indicate fluctuations, while tildes and double primes indicate Favre averages and their fluctuations: $X = \overline{X} + X' = \widetilde{X} + X'' = \overline{\rho X}/\overline{\rho} + X''$.

The governing equations for HBT are derived using two transformations. The first was used for SRT:

$$t^* = t, \quad x_i^* = x_i \left(\frac{h(t_o)}{h(t)}\right)^{\delta_{i1}}, \quad \hat{u}_i = u_i \frac{h'(t_o)}{h'(t)} \tag{6}$$

where h is a measure of the mixing layer height, t_o is an arbitrarily chosen instant in time, and δ_{ij} is the Kronecker delta function. The vertical direction corresponds to the index 1. The transformation represents a rescaling by the expected self-similar growth of lengthscales and velocity scales.

A second transformation is then applied:

$$\rho^* = \rho \frac{\overline{\rho}(x_o,t_o)}{\overline{\rho}(x_1,t_o)}, \quad u_i^* = \left(\hat{u}_i - \frac{\overline{\rho \hat{u}_1}}{\overline{\rho}}\right)\left(\frac{\overline{\rho}(x_1,t_o)}{\overline{\rho}(x_o,t_o)}\right)^{1/2},$$
$$Y^* = Y \frac{\overline{\rho}(x_1,t_o)}{\overline{\rho}(x_o,t_o)}, \quad p^* = p - \overline{p}(x_1,t_o) \tag{7}$$

x_o is the vertical location of the midplane, defined as where $\mathrm{d}[\overline{\rho u_1}(x_1,t_o)]/\mathrm{d}x_1 = 0$. This transformation removes the mean gradients in ρ^* and p^* at the midplane while retaining a near-zero mean gradient in $\overline{\rho^* \hat{u}^{*2}_i}$. This is to maximize the homogeneity of the variables in the vicinity of the midplane.

These transformations are substituted together into the TRT equations, then evaluated near $t^* = t_o$, and $x_1^* = x_o$, such that $h(t) \approx h(t_o)$, $h'(t) \approx h'(t_o)$, and $\overline{\rho}(x_1,t_o) \approx \overline{\rho}(x_o,t_o)$. This results in a set of equations identical to TRT but with additional source terms. One source term appears in the continuity equation, but it is found to vanish at high Reynolds number and is neglected. The kinetic energy equation becomes:

$$\begin{aligned}\frac{\partial \overline{\rho^*}\widetilde{k^*}}{\partial t^*} = & \underbrace{-\frac{\partial \frac{1}{2}\overline{\rho^*}\widetilde{u_i^{*2} u_j^*}}{\partial x_j^*} - \frac{\partial \overline{u_j^* p^*}}{\partial x_j^*}}_{I} \underbrace{+ \overline{p^* \frac{\partial u_i^*}{\partial x_i^*}}}_{II} \underbrace{- \overline{\rho^*}\widetilde{\varepsilon^*}}_{III} \\ & \underbrace{+ \frac{\partial \overline{u_i^* \tau_{ij}^*}}{\partial x_j^*}}_{IV} \underbrace{+ g\overline{\rho^{*\prime} u_1^{*\prime}}}_{V} \underbrace{- \frac{1}{2\tau_o}\overline{\rho^*}\widetilde{u_i^{*2}}}_{VI} \underbrace{- \overline{u_1^*}\frac{\mathrm{d}\overline{p}}{\mathrm{d}x_1^*}}_{VII} \\ & \underbrace{+ \overline{u_i^* \frac{\partial \tau_{ij} - \tau_{ij}^*}{\partial x_j^*}}}_{VIII} \underbrace{+ \frac{\widetilde{u}_1 \overline{\rho^*}\widetilde{k^*}}{\lambda_o}}_{IX} \underbrace{+ \frac{\widetilde{u}_1 \overline{\rho^*}\widetilde{u_1^{*2}}}{\lambda_o}}_{X} \underbrace{+ \frac{\overline{\rho^*}\widetilde{u_1^* u_i^{*2}}}{4\lambda_o}}_{XI}\end{aligned} \tag{8}$$

where k is the kinetic energy, ε is the viscous dissipation rate, $\tau_o = h(t_o)/h'(t_o)$ is the characteristic timescale of the TRT layer growth at $t = t_o$, and $\lambda_o = \overline{\rho}(x_o,t_o)/(\mathrm{d}\overline{\rho}/\mathrm{d}x_1)|_{x_o,t_o}$ is the characteristic lengthscale of the density variation at $x_1 = x_o$ and $t = t_o$.

Similarly, the scalar variance equation becomes:

$$\begin{aligned}\frac{\partial \overline{Y^{*\prime 2}}}{\partial t^*} = & \underbrace{-\overline{u_1^*}\frac{\partial \overline{Y^{*\prime 2}}}{\partial x_1^*}}_{I} \underbrace{- \frac{\partial \overline{u_1^{*\prime} Y^{*\prime 2}}}{\partial x_1^*}}_{II} \underbrace{+ 2\overline{u_1^{*\prime} Y^{*\prime}}\frac{\partial \overline{Y^*}}{\partial x_1^*}}_{III} \\ & \underbrace{-2\chi^*}_{IV} \underbrace{+ D\frac{\partial^2 \overline{Y^{*\prime 2}}}{\partial x_1^{*2}}}_{V} \underbrace{+ 2D\overline{Y^{*\prime}\left(\frac{1}{\rho^*}\frac{\partial \rho^*}{\partial x_j^*}\frac{\partial Y^*}{\partial x_j^*}\right)}}_{VI} \\ & \underbrace{-2D\overline{Y^{*\prime 2}}\frac{\partial}{\partial x_j^*}\left(\frac{1}{\overline{\rho}}\frac{\partial \overline{\rho}}{\partial x_1^*}\right)}_{VII} \underbrace{+ 2\frac{(\overline{u_1^*} + \widetilde{u}_1)\overline{Y^{*\prime 2}}}{\lambda_o}}_{VIII} \underbrace{+ 2\frac{\overline{u_1^{*\prime} Y^{*\prime} Y^*}}{\lambda_o}}_{IX}\end{aligned} \tag{9}$$

where χ is the viscous dissipation rate.

Figure 1 (*a*, *b*) gives the normalized values of the kinetic energy and scalar variance budget terms at the midplanes of

SRT DNS, plotted against Reynolds number. Terms consistently less than 1% of buoyant production (term V) in figure 1 (*a*), or less than 1% of mean gradient production (term IX) in figure 1 (*b*), are omitted. All terms appear insensitive to Reynolds number. Terms IX, and X, and XI in the kinetic energy budget, along with terms III and VI in the scalar variance budget, are each less than 5% of the buoyant production, and so can be neglected. The turbulent and pressure transport (term I) in the kinetic energy budget and the turbulent scalar transport (term II) in the scalar variance budget, each arise from residual inhomogeneity in the transformed variables, and so cannot be included directly in HBT.

Of the source terms resulting from the transformations, only two have significant contributions (term VI, the layer growth term, for kinetic energy and term IX, the mean gradient production, for scalar variance), so only these terms are retained explicitly in the HBT governing equations:

$$\frac{\partial \rho^*}{\partial t^*} + \frac{\partial \rho^* u_j^*}{\partial x_j^*} = 0, \tag{10}$$

$$\frac{\partial \rho^* u_i^*}{\partial t} + \frac{\partial \rho^* u_i^* u_j^*}{\partial x_j^*} = -\frac{\partial p^*}{\partial x_i^*} + \frac{\partial \tau_{ij}^*}{\partial x_j^*} + g\rho^{*'}\delta_{1i} - \frac{1}{2\tau_o}\rho^* u_i^*, \tag{11}$$

$$\frac{\partial \rho^* Y^*}{\partial t} + \frac{\partial \rho^* Y^* u_j^*}{\partial x_j^*} = \frac{\partial}{\partial x_j^*}\left(\rho^* D \frac{\partial Y^*}{\partial x_j^*}\right) + \frac{u_1^{*'}}{\alpha \lambda_o}, \tag{12}$$

where the final terms in the momentum and scalar equations arise from the layer growth and mean gradient production terms, respectively.

Equations (10)-(12) thus govern a flow which is stationary, on account of the transformation of Eq. (6), approximately homogeneous, on account of the transformation of Eq. (7), and representative of an RT instability in the vicinity of $t = t_o$ and $x_1 = x_o$. When implemented in a periodic box, they produce a stationary homogeneous flow whose small scales model the small scales of the TRT midplane. Because global quantities like the bulk Reynolds and Atwood number are not defined in the HBT configuration, it is instead parameterized by two local statistics, the turbulent Reynolds number and an effective Atwood number:

$$\mathrm{Re_t} = \frac{\widetilde{k}^2}{\nu\widetilde{\varepsilon}}, \qquad \mathrm{At_{eff}} = \frac{\overline{\rho'^2}^{1/2}}{\overline{\rho}} \tag{13}$$

NUMERICAL IMPLEMENTATION

The HBT Eqs. (10)-(12) are implemented in DNS with triply periodic box boundary conditions. To close the equations, the parameters τ_o, λ_o, and g must be specified.

To determine τ_o, it is noted that in figure 1 (*a*) the ratio between the layer growth term VI and the viscous dissipation term III is approximately constant with Reynolds number. This implies that the ratio between the turbulence timescale $\tau_t = \overline{k}/\overline{\varepsilon}$ and τ_o is a constant (≈ 0.41) in the self-similar limit. At each timestep in HBT, the instantaneous value of τ_t is calculated in terms of volume averages, then the constant ratio is enforced to define τ_o. Because this ensures that the ratio of layer growth to dissipation in the HBT kinetic energy budget adheres to the value observed in SRT, deviation of the HBT energy dynamics from SRT due to neglected terms in Eq. (8) manifests as a reduction in the buoyant production; likewise, neglected terms in the scalar variance budget emerge as a reduction in the mean gradient production.

Rather than prescribing constant values for g and λ_o, constant rates of kinetic energy and scalar variance injection, P_g and P_λ, are imposed on the gravity and mean gradient terms in the momentum and scalar transport equations. The modified terms take the forms:

$$g\rho^{*'} \to -\overline{\rho^*}P_g \frac{\rho^{*'}}{|\langle \rho^{*'} u_1^{*'}\rangle|}, \quad \frac{u_1^{*'}}{\alpha\lambda_o} \to \overline{\rho^*}P_\lambda \frac{u_1^{*'}}{|\langle u_1^{*'} Y^{*'}\rangle|} \tag{14}$$

Where angle brackets indicate volume averages. This modification, inspired by a similar modification used for linear forcing in homogeneous isotropic turbulence (Rosales & Meneveau, 2005; Carroll & Blanquart, 2013), has the effect of reducing temporal fluctuations in HBT, reducing the amount of data necessary to obtain converged statistics through time-averaging.

The finite difference solver NGA (Desjardins *et al.*, 2008) is used to solve the conservative form of the HBT Eqs. (10) - (12). The reader is referred to Desjardins *et al.* (2008) for full details of the numerical methods used.

VERIFICATION OF HBT PROPERTIES

Figure 2 shows density fields for both the TRT DNS case of Goh & Blanquart (2025) and the R4 case of HBT. The TRT clearly shows the heavy and light fluid ($\rho_H = 3\rho_L$) reservoirs at the top and bottom of the domain, with a highly turbulent region of high density variance at the center. The HBT field, despite lacking the reservoirs, maintains a similar degree of density variance via the mean gradient term in Eq. (12), with the density fluctuating more than 40% above and below the mean value. The insets at the center of Figure 2 illustrate the modeling capability of HBT. A small region near the midplane of the Goh & Blanquart (2025) TRT is seen to resemble a region of the HBT.

In order to verify the statistical stationarity of HBT and examine of the effect of the modifications of Eq. (14), Figure 3(*a*, *b*) shows the density-weighted volume averages for two cases of HBT, plotted against time. These are shown alongside midplane data of a corresponding SRT case. Qualitatively, the simulations appear stationary in time after a short transient evolution, visible in the inset of figure 3(*a*). The modification not only succeeds in reducing the magnitude of the temporal fluctuations, but also improves their fidelity by bringing them further in line with SRT data, which has far smaller fluctuations than HBT with the unmodified forcing.

To determine whether the cascade dynamics in HBT accurately represent SRT and TRT, the 2D spectral budgets of kinetic energy and scalar variance of both an HBT case and an SRT case have been plotted in Figure 4 (*a*, *b*). These are calculated by taking the 2D Fourier transform (in the horizontal directions) of the momentum and scalar equations, multiplying by the conjugate of the Fourier transforms of the velocity and scalar, taking the real part, then integrating around annuli of constant wavenumber in wave vector space.

The terms of HBT and SRT nearly collapse at all but the smallest four wavenumbers, demonstrating that the small-scale time dynamics of SRT and TRT turbulence is captured by HBT. The errors in the large scales are limited to the convection, pressure, and buoyant production in the kinetic energy budget, and to the convection and mean gradient production in

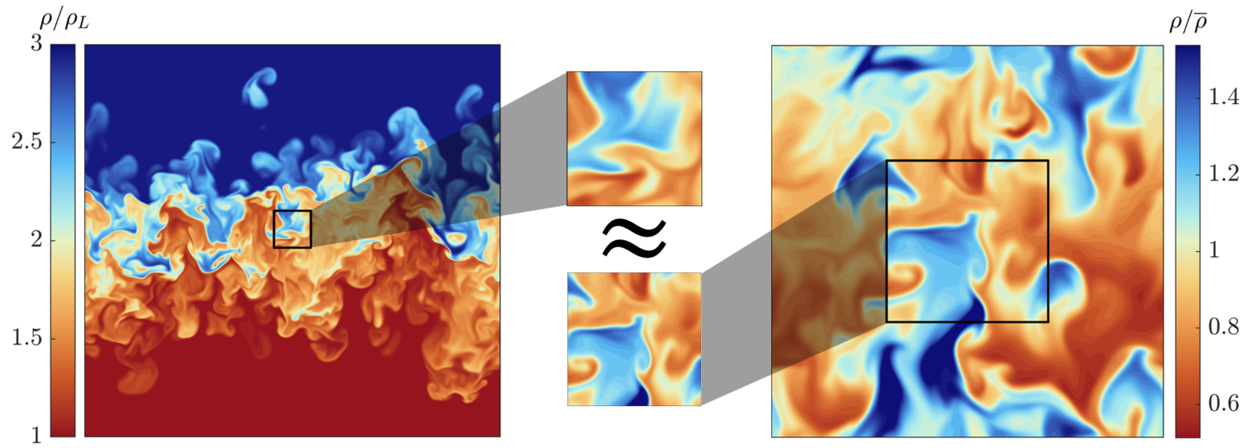

Figure 2: Density fields for TRT (left) and HBT (right). For the TRT, $\mathrm{Re} \approx 6400$, $\mathrm{At} = 0.5$. For the HBT, $\mathrm{Re_t} = 1090$, $\mathrm{At_{eff}} = 0.28$.

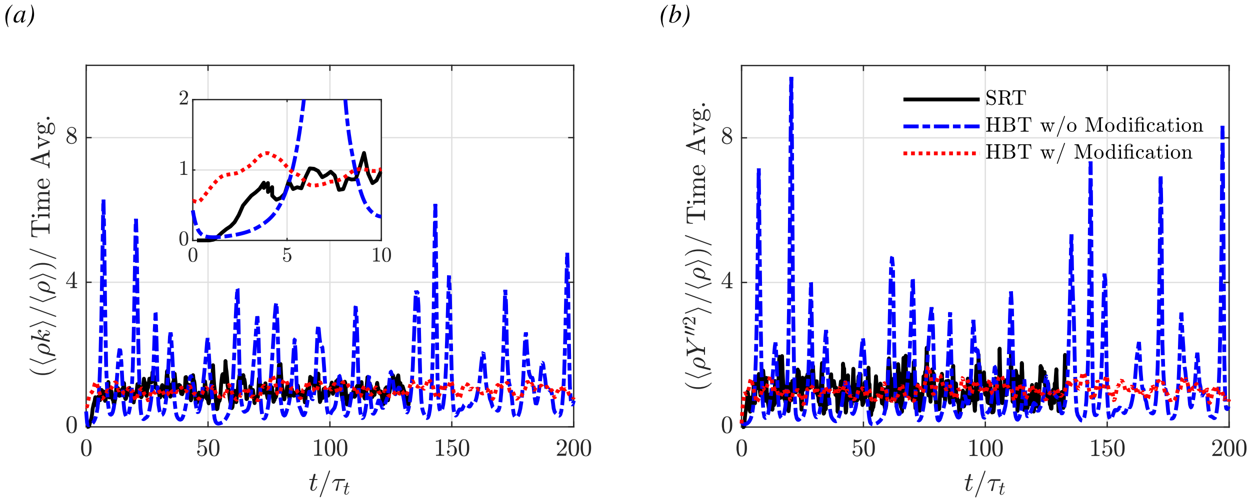

Figure 3: Time series data for the density-weighted volume averages of (*a*) the turbulent kinetic energy and (*b*) the scalar variance for HBT ($\mathrm{Re_t} = 200, \mathrm{At_{eff}} = 0.28$), with and without the source term modification, and SRT ($\mathrm{Re_t} = 240$, $\mathrm{At_{eff}} = 0.23$ at midplane). Values are normalized by the time-average.

the scalar variance budget. This is expected, as the convection and pressure terms in the kinetic energy equation of SRT include the pressure transport, turbulent transport, and other terms neglected in HBT, which, as stated earlier, emerge in HBT as a reduction in the buoyant production. The same is true for the convection of the scalar variance budget, where the neglected terms emerge in HBT as a reduction in the mean gradient production.

COMPARISON OF HBT TO TRT

To validate HBT's ability to model high-Reynolds number TRT, HBT cases are compared to the TRT DNS of Cabot & Cook (2006).

Figure 5 (*a*) shows probability density functions (PDF) of the normalized density for both TRT and HBT. The PDFs share the same qualitative shape: a skewed bell curve. Differences between the TRT and HBT distributions are small enough over most of the distribution to be attributed to statistical fluctuations. Noteworthy differences appear only near the edges of the distributions; while HBT smoothly decays to zero at both ends, the TRT distributions spike upward then stop at distinct limits. These two limits correspond to the properties of pure heavy/light fluids. The violation of these bounds in HBT arises from the introduction of a source term to the scalar transport Eq. (12). Since the discrepancies are limited to the fringes of the distribution, which account for only a small fraction of the total fluid mass, HBT's overall fidelity seems to have not been harmed by the loss of imposed scalar bounds.

Figure 5 (*b*) shows variances of components of the velocity gradient tensor $\partial u_i/\partial x_j$ across x_1 for TRT, overlain with HBT values. The ratios of components and their departure from isotropic values is nearly identical between TRT and HBT. This indicates that the degree of anisotropy in the velocity field is similar between the two frameworks, especially at the small scales. Moreover, the gradient variances are nearly constant across the layer so that, by this metric, HBT remains representative of TRT beyond just the midplane location.

Figure 6 (*a*) shows the 2D spectra, where E_{ii}^{2D} is the 2D spectrum of u_i, of the vertical and horizontal velocity at the midplane of TRT, overlain with the spectra of HBT, while 6 (*b*) gives the spectral anisotropy:

$$B = \frac{E_{11}^{2D}}{E_{11}^{2D} + E_{22}^{2D} + E_{33}^{2D}} - \frac{1}{3} \qquad (15)$$

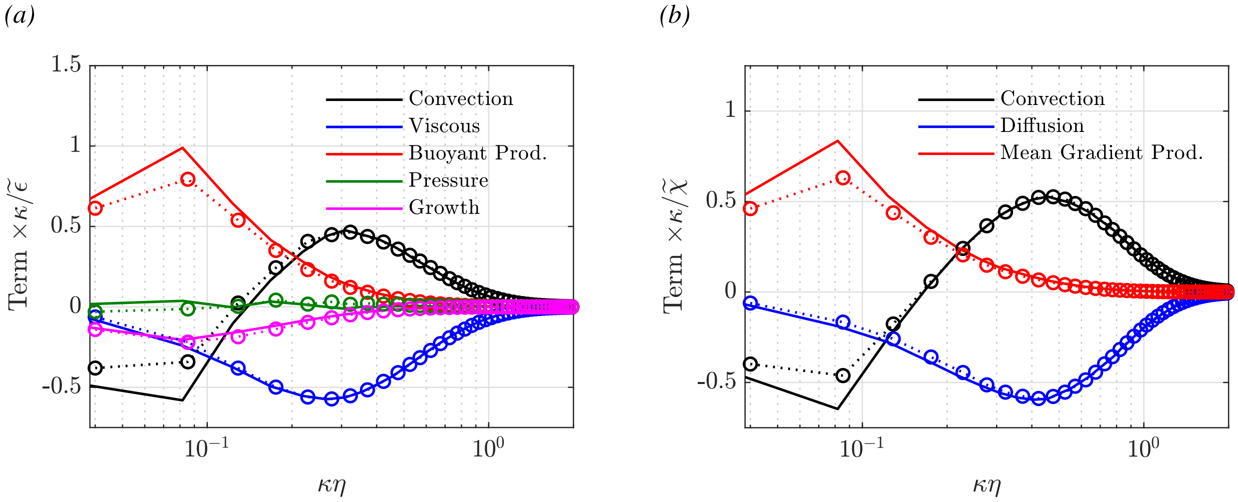

Figure 4: 2D spectral budgets for (*a*) kinetic energy and (*b*) scalar variance for the midplane of SRT ($\mathrm{Re_t} = 350$, $\mathrm{At_{eff}} = 0.23$ at midplane; solid lines) and HBT ($\mathrm{Re_t} = 350$, $\mathrm{At_{eff}} = 0.27$; dotted lines). Terms are multiplied by κ for visibility.

for HBT alongside its range of fluctuations in TRT. Except at the lowest HBT wavenumber, the results for the two configurations collapse within statistical fluctuations for both the vertical and horizontal components, and the HBT anisotropy spectrum remains within the range of TRT fluctuations at nearly all wavenumbers. Thus, HBT captures both the spatial structure of the TRT velocity field and the anisotropy between velocity components across almost all lengthscales.

Figure 7 (*a*) gives the density 2D spectra, $E^{2D}_{\rho\rho}$, for TRT and HBT, while Figure 7 (*b*) gives the spectral coherence between the vertical velocity and density:

$$r_{1\rho} = \frac{E^{2D}_{1\rho}}{(E^{2D}_{11} E^{2D}_{\rho\rho})^{1/2}} \tag{16}$$

for HBT, with the range of fluctuations for TRT. $E^{2D}_{1\rho}$ is the 2D cospectrum of u_1 and ρ. The density spectra collapse within statistical fluctuations and the HBT coherence remains within the range of TRT fluctuations at all but the lowest wavenumber. Thus, HBT captures not only the spatial variation of density, but also the correlation of this variation with vertical velocity, responsible for kinetic energy production through buoyancy.

The HBT spectra's fidelity to TRT, despite occupying a smaller range of wavenumbers, illustrates HBT's ability to decouple the small-scale TRT turbulence from large-scale structures. Notably, HBT is able to achieve this agreement with a grid size of 320^3 compared to TRT's 3072^3, demonstrating significant computational savings.

CONCLUSION

The HBT framework for modeling TRT turbulence in a stationary homogeneous flow is presented. Using variable transformations, two source terms are derived to produce turbulence in a triply periodic box. The resulting flow successfully models the small-scales of TRT turbulence, including cascade dynamics, PDFs, anisotropy, and turbulence spectra, while avoiding a large, costly computational grid. We foresee that HBT will lead to greater physical insight into Rayleigh-Taylor instabilities and will assist as an inexpensive a priori and a posteriori test bed in the development of buoyancy-focused subgrid-scale models.

ACKNOWLEDGEMENTS

This material is based upon work supported by the National Science Foundation under Grant No. 2422513 and the National Science Foundation Graduate Research Fellowship Program under Grant No. 2139433. Any opinions, findings,and conclusions or recommendations expressed in this material are those of the author(s) and do not necessarily reflect the views of the National Science Foundation.

REFERENCES

Cabot, W.H. & Cook, A.W. 2006 Reynolds number effects on Rayleigh–Taylor instability with possible implications for type-Ia supernovae. *Nat. Phys.* **2**, 562 – 568.

Carroll, P.L. & Blanquart, G. 2015 A new framework for simulating forced homogeneous buoyant turbulent flows. *Theor. Comput. Fluid Dyn.* **29** (3), 225–244.

Carroll, Phares L. & Blanquart, G. 2013 A proposed modification to lundgren's physical space velocity forcing method for isotropic turbulence. *Physics of Fluids* **25** (10).

Chung, D. & Pullin, D.I. 2010 Direct numerical simulation and large-eddy simulation of stationary buoyancy-driven turbulence. *J. Fluid Mech.* **643**, 279–308.

Desjardins, O., Blanquart, G., Balarac, G. & Pitsch, H. 2008 High order conservative finite difference scheme for variable density low Mach number turbulent flows. *J. Comput. Phys.* **227** (15), 7125–7159.

Goh, Chian Yeh & Blanquart, Guillaume 2025 A statistically stationary minimal flow unit for self-similar rayleigh–taylor turbulence in the mode-coupling limit. *Journal of Fluid Mechanics* **1002**.

Livescu, D. & Ristorcelli, J. R. 2007 Buoyancy-driven variable-density turbulence. *Journal of Fluid Mechanics* **591**, 43–71.

Ristorcelli, J. R. & Clark, T. T. 2004 Rayleigh–taylor turbulence: self-similar analysis and direct numerical simulations. *Journal of Fluid Mechanics* **507**, 213–253.

Rosales, Carlos & Meneveau, Charles 2005 Linear forcing in numerical simulations of isotropic turbulence: Physical space implementations and convergence properties. *Physics of Fluids* **17** (9).

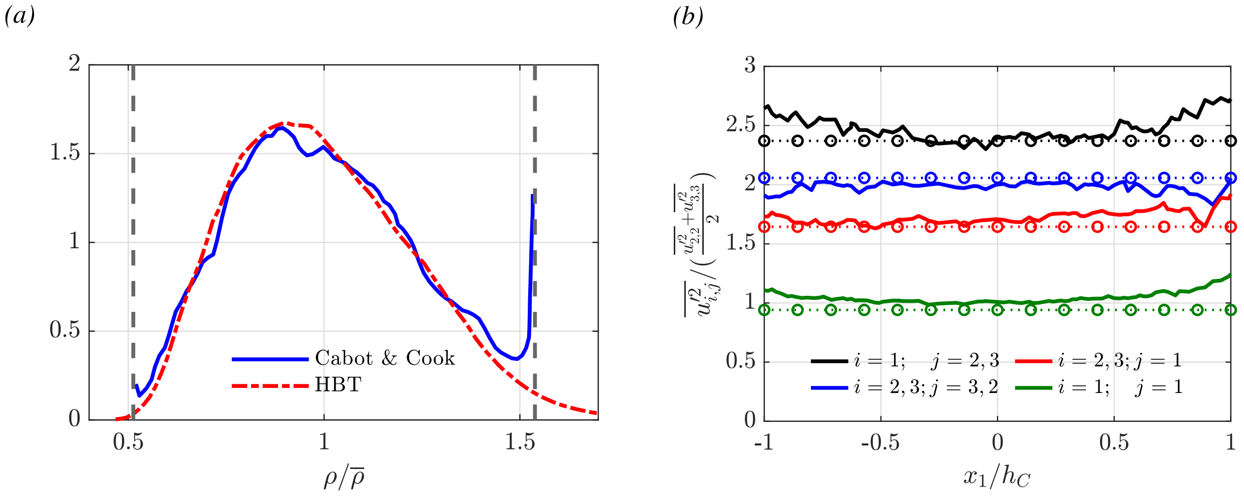

Figure 5: (*a*) PDFs for the density, normalized by its mean, and (*b*) variances of the velocity gradient tensor, normalized by the variance of the longitudinal derivative of horizontal velocity. Data is shown for the Cabot & Cook (2006) TRT ($\mathrm{Re_t} \approx 2000$, $\mathrm{At_{eff}} = 0.23$ at midplane) and HBT ($\mathrm{Re_t} = 2010$, $\mathrm{At_{eff}} = 0.24$)

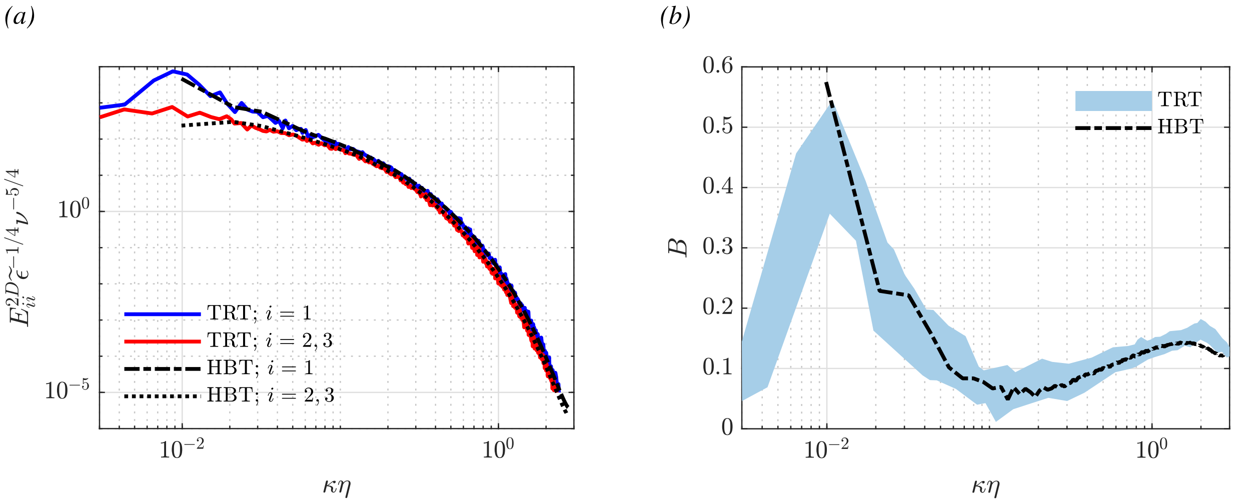

Figure 6: (*a*) 2D velocity spectra for the midplane of the Cabot & Cook (2006) TRT ($\mathrm{Re_t} \approx 3500$, $\mathrm{At_{eff}} = 0.23$), and HBT ($\mathrm{Re_t} \approx 3360$, $\mathrm{At_{eff}} = 0.24$) normalized by $\widetilde{\varepsilon}$ and ν, and (*b*) spectral anisotropy of the velocity field.

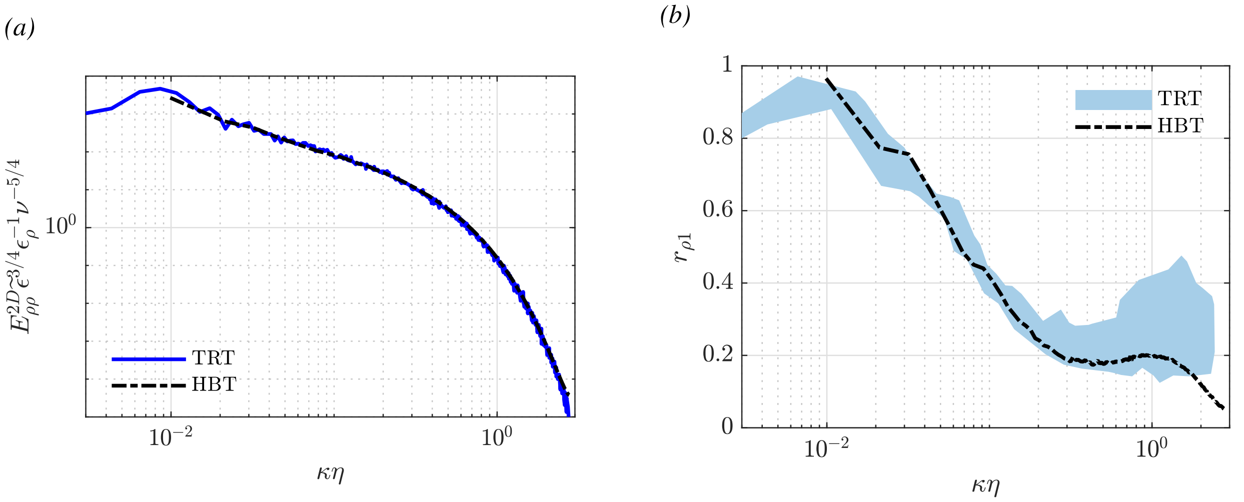

Figure 7: (*a*) 2D velocity spectra for the midplane of the Cabot & Cook (2006) TRT and HBT (same parameters as above) normalized by $\widetilde{\varepsilon}$, $\widetilde{\varepsilon}_\rho = D(\partial\rho/\partial x_j)^2$, and ν, and (*b*) spectral coherence of the vertical velocity and density fields